

microARPES and nanoARPES at diffraction-limited light sources: opportunities and performance gains

Eli Rotenberg* and Aaron Bostwick

Advanced Light Source, MS 6-2100, E. O. Lawrence Berkeley National Laboratory, Berkeley, CA 94720, USA. *E-mail: erotenberg@lbl.gov

Received 24 April 2014

Accepted 1 July 2014

The scientific opportunities for microARPES and nanoARPES techniques are discussed, and the benefits to these techniques at diffraction-limited light sources are presented, in particular the impact on spectromicroscopic ARPES (angle-resolved photoemission spectroscopy) of upgrading the Advanced Light Source to diffraction-limited performance. The most important consideration is whether the space-charge broadening, impacting the energy and momentum resolution, will limit the possible benefits for ARPES. Calculations of energy broadening due to space-charge effects will be presented over a wide range of parameters, and optimum conditions for ARPES will be discussed. The conclusion is that spectromicroscopic ARPES will greatly benefit from the advent of diffraction-limited light sources; space-charge broadening effects will not be a limiting factor.

© 2014 International Union of Crystallography

Keywords: ARPES; nanoARPES; photoemission; space-charge broadening.

1. Introduction: ARPES

Angle-resolved photoemission spectroscopy, or ARPES, is a preeminent tool for determining the electronic structure of solids. At its simplest, ARPES is a measurement of the response of a solid to the removal of one electron by one photon. Fig. 1 illustrates a typical experimental set-up (Rotenberg, 2010). The photons from a light source impinge on a sample in an ultrahigh-vacuum (UHV) environment. The photons that are absorbed by the sample generate a large number of photoelectrons, some of which are collected by an electron lens, dispersed through an electron spectrometer (here a hemispherical deflection is used), and counted by some kind of detector (typically an imaging channel-plate type).

ARPES is based on the photoelectric effect, in which a photon of incident energy $h\nu$ induces emission of an electron of kinetic energy (KE). The relationship between these is just given by conservation of energy as

$$\text{KE} = h\nu - \text{BE} - \Phi, \quad (1)$$

where Φ is the work function of the material and BE is the binding energy of the electron.

In ARPES, we are concerned not only about the energies of the particles but also their momenta. This is determined by applying not only equation (1) but also conservation of momentum relations (Kevan, 1992; Hüfner, 1996). These relations should be approached with caution, however, because they make assumptions about the emission process that may not be true in general. Nevertheless, these assumptions appear to be justified on the grounds that, for simple systems like carbon, tungsten, copper and silicon, ARPES has

spectacularly confirmed the predicted electronic band structure.

ARPES works well not only for simple materials but also for new complex materials of fundamental and practical interest. There are three relevant kinds of complexity of interest in materials: firstly, in *correlation*, or the interaction between the internal degrees of freedom; secondly, in the

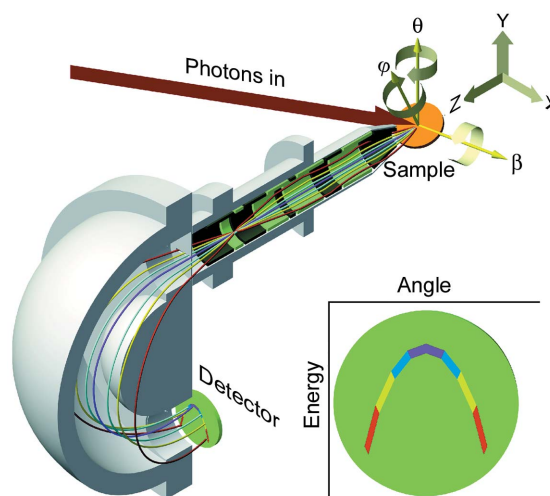


Figure 1 ARPES schematic. Incident photons excite a distribution of photoelectrons at the sample. The photoelectrons in a plane are dispersed in energy and angle by a combination of an electron lens coupled to a hemispherical capacitor. Electrons with a range of energy and angles are directly imaged onto a two-dimensional multi-channel detector. A sample goniometer allows for the XYZ and angular positioning of the sample with respect to the detector and incident photon beam. [Reproduced from Rotenberg (2010).]

organization of the constituent components of the material, and, thirdly, when there is an interplay between correlation and organization. The effects of correlation have been the major focus of ARPES for the last 20 years, driving significant improvements in the energy resolution and efficiency of detectors.

Studies of the organizational aspects have also received much attention. This organization is reflected for example by the arrangement of constituent materials in multi-layered engineered heterostructures, leading to quantum confinement effects on the electronic structure (Chiang, 2000). Historically, the available X-ray spot sizes, typically in the micrometer to millimeter range, have been much larger than the relevant length scales for confinement. So such organizational effects have been limited to surface and thin film effects, where the limited penetration depth of the ARPES probe (typically nanometers) has been employed to study quantum size effects in one direction of samples that are homogeneous in the plane.

Most interesting is the third kind of complexity, in which correlation and organization effects are interrelated. One common example is the self-organization of materials into electronic or magnetic domains. Both of these material organizations can take place on length scales from the micrometer to the nanometer, and furthermore there is an interplay between these externally and internally derived length scales. In a grand scheme, by influencing this interplay, we can hope to control not only how electrons move in a solid but also the energy conversion between electronic and other propagating modes such as vibrational, magnetic and optical waves.

For example, since electrons and phonons have different length scales, the electron–phonon interaction will certainly be influenced when samples are reduced to lengths comparable with the typical phonon wavelength (Valla *et al.*, 2000). This leads to the possibility of controlling many-body interactions, for the purpose, for example, of controlling superconductivity or other exotic ground states.

These issues are tied to the concept of *emergent* phenomena in complex systems, the idea that in multi-particle systems, as the system size increases from the atomic to the mesoscopic, the interplay of space, time, charge, spin *etc.* degrees of freedom lead to new behaviors that cannot easily be predicted from microscopic principles, from the bottom up. Here, a particle has to be taken in a very general sense, in which not only electrons and nuclei but also excitations such as photons, phonons, magnons, charge density waves are considered. Mesoscopic science is considered a forefront issue in condensed matter systems and is likely to be avidly studied in the coming years (Hemminger *et al.*, 2012).

ARPES can provide critical information on these many-body interactions (Damascelli, 2004; Kaminski & Fretwell, 2005). Assuming that the emitted electrons leave the solid quickly enough, then their observed spectral linewidth, in energy and momentum, relate directly back to the lifetime of the excited solid that is left behind. This excited state consists of an ensemble of $\sim 10^{23}$ electrons, minus the one we removed. But what is remarkable is that this ensemble can very often be

treated as a single, positive particle called the ‘hole’ left behind, and that the interactions between these holes and the other bodies in the system can be treated as though the hole is a point particle which propagates as a ‘real’ particle. This is the quasiparticle approximation, and ARPES data contain critical information about the lifetime and renormalized energies of these quasiparticles.

The interpretation of the ARPES data in terms of many-body interactions has been reviewed by Damascelli & Shen (2003) and the essentials are reproduced here. The propagation of quasiparticles is described by a complex function called the self-energy Σ ,

$$\Sigma(\mathbf{k}, \omega) = \Sigma'(\mathbf{k}, \omega) + i\Sigma''(\mathbf{k}, \omega), \quad (2)$$

whose real and imaginary function parts describe the renormalization of the quasiparticle’s lifetime and energy relative to the non-interacting system. Here \mathbf{k} is the quasiparticle momentum, and ω is the quasiparticle energy, expressed in units of eV when $\hbar = 1$. This function Σ is analogous to the complex index of refraction n that describes the passage of photons through a medium, and, like n , Σ is derived from the dielectric response function of the medium. In a system characterized without interactions by the ‘bare’ band structure $\omega_b(\mathbf{k})$, ARPES measures the spectral function

$$A(\mathbf{k}, \omega) = -\frac{1}{\pi} \frac{\Sigma''(\mathbf{k}, \omega)}{[\omega - \omega_b(\mathbf{k}) - \Sigma'(\mathbf{k}, \omega)]^2 + \Sigma''(\mathbf{k}, \omega)^2}, \quad (3)$$

modulated by a Fermi cut-off function at the Fermi level ($\omega = E_F = 0$). In an ARPES measurement, the spectral function $A(\mathbf{k}, \omega)$ is further modulated by optical matrix elements which give information of the symmetry of wavefunctions probed.

As an example, Fig. 2 shows calculations of the spectral function of graphene, a single layer of carbon atoms arranged in a honeycomb lattice, which is the basis of graphite, C_{60} , carbon nanotubes and other sp^2 forms of carbon, based on different contributions to the self-energy (Bostwick *et al.*, 2010). The bare bandstructure, shown in Fig. 2(b) for electron-doped graphene, famously consists of two linear bands, which cross at the so-called Dirac energy E_D .

When the electrons interact with optical phonons (at around $\omega_0 = 180$ meV in graphene), the computed spectral function (Fig. 2b) shows that the lifetime of the quasiparticles is dramatically decreased (the spectrum becomes broader) for quasiparticles with energy $|\omega| > \omega_0$. This decreased lifetime is due to scattering of the quasiparticle accompanied by emission of an optical phonon, which is kinematically forbidden for quasiparticles of energy $|\omega| < \omega_0$. But it should be noted that all quasiparticles are affected by the electron–phonon interaction regardless of energy because of the necessarily non-zero term Σ' in equation (3). Whereas Σ'' in our example is a simple step function, zero in a finite range near $\omega = 0$, Σ' , related to the latter by Kramers–Kronig transformation, is non-zero at nearly all energies. This leads to a shift in the energy band away from the bare band energies, that causes the observed band to be *kinked*.

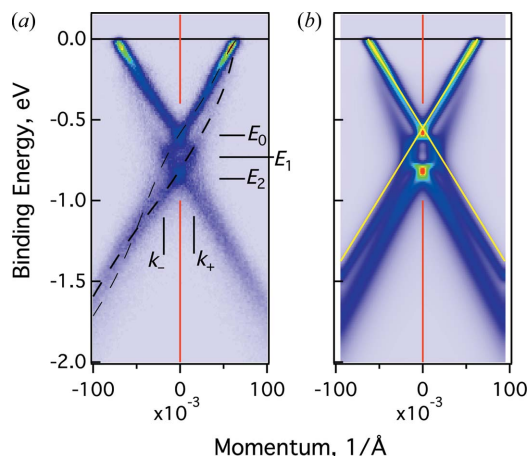


Figure 2 Experimental (a) and theoretical (b) spectral function of doped graphene. The bare band structure in this cut of momentum space [yellow lines in (b)] consists of two linear bands crossing at a single point, the so-called Dirac crossing. The actual ARPES spectral function in (a) is far more complicated, consisting of four branches (two indicated by black dashed lines) indicating that there are multiple excitations created by the ARPES optical transition. These modes are described as propagating holes either undressed or dressed with plasmons. Ultimately these modes are a consequence of the electron–electron interaction as predicted by GW theory in (b). [Results adapted from Bostwick *et al.* (2010). *Science*, **328**, 999–1002. Reprinted with permission from AAAS.]

The quasiparticles are observed at the zeros of the first term in the denominator of equation (3). For simple self-energy functions, this amounts to weak deviations of the quasiparticle from the bare bands, such as the kinks mentioned above. The electron–electron interaction can lead to more complicated self-energy functions; when the self-energy Σ' is sufficiently oscillatory, then multiple poles of the spectral function $A(\mathbf{k}, \omega)$ can occur at a given momentum. This reflects the emergence of new charged quasiparticles in the observed ARPES spectral function. One such example occurs when the quasiparticle decay into plasmons is considered. Plasmons are a collective oscillation of the electron gas in a metal, and dominate the long-range Coulomb interaction. Fig. 2 shows the measured (a) and computed (b) spectral function for graphene when this interaction is accounted for (Bostwick *et al.*, 2010). Now, each band is split into two, one being an ordinary quasiparticle, the other being a quasiparticle ‘dressed’ with a plasmon. Such a composite particle is called a plasmaron (Lundqvist, 1967a,b, 1968).

2. Why diffraction-limited sources?

There are particular advantages to performing ARPES at synchrotrons, namely high flux, high brightness and wide tunability. Of these, increased brightness is the primary improvement available at diffraction-limited (DL) light sources, with three principal advantages discussed below.

Advantage 1. At the diffraction limit, the focusing of the monochromated light can be optimized to wavelength-limited spatial resolution. This means that small samples can be studied in spectromicroscopy schemes. MAESTRO, a state-of-the-art ARPES beamline based on a variable-line-space

plane-grating monochromator design (Hu *et al.*, 2007; Warwick & Reininger, 2010), consists of two ARPES end-stations. Considering the improved focus after an upgrade to DL performance, these end-stations can achieve up to a factor of six improvement in flux for the same spot size. This is because, in simple terms, in the current operating mode of the ALS, the flux-restricting apertures are overfilled by about this factor.

Advantage 2. Through advances such as on-axis injection, it is now possible to reduce the size of the vacuum chamber containing the beam. Therefore it becomes possible to build insertion devices (IDs) not only with smaller gaps (and commensurately higher magnetic field), but new four-fold symmetric insertion devices become possible, which can generate yet higher magnetic fields. [A good example of such an insertion device is the Delta device developed at Cornell (Temnykh, 2008).] With both stronger magnetic fields and smaller gap, IDs can have a shorter period for a similar energy range. Given that the coherent undulator flux goes as the square of the number of periods, the coherent flux can be greatly improved in this way. A reasonable estimate is that an enhancement of flux by a factor of three or four should be possible.

This leads to an important economic impact. Smaller IDs have simpler movement mechanisms, leading to cost savings. But, more importantly, storage rings with either short straight sections, or (like the ALS) long straight sections that are chicaned for two insertion devices, can in some cases remain competitive with facilities having longer straight sections. This translates into either less expensive or increased number of beamlines. It should be noted that the useful flux for ARPES is limited by space-charge effects (see §3 below), so it is not clear that, with respect to ARPES, there is any advantage to insertion devices with lengths longer than a couple of meters or so even at new DL light sources.

Advantage 3. Whenever the source size is reduced, as is possible at DL light sources, there are advantages for the monochromator design, whereby the small source leads to more efficient systems with higher energy resolution. A similar advantage is found in the detector side, where the small source (here the photoemission volume at the sample) leads to improved performance (improved energy and momentum resolution of the detected electrons) even with today’s existing detectors.

Therefore, at DL light sources, the improved energy and spatial resolutions go hand in hand to improve the ARPES technique. These advantages for ARPES are discussed in the next sections.

2.1. Energy resolution

As summarized in Table 1, the required energy resolution for ARPES depends on the energy scale of the interactions which are being targeted. Merely observing the band structure, largely derived from lattice symmetry and chemical interactions, is the least demanding situation for ARPES, and so moderate energy resolution on the order of 100 meV is more than adequate. Similarly, the exchange splitting in

Table 1

Energy resolution regimes for ARPES.

Physics	Desired energy resolution
Chemical state	100–500 meV
Magnetism	50–500 meV
Electron–phonon coupling	5–50 meV
Electron–electron correlation	1–20 meV
High- T_c superconductivity	<30 meV
Low- T_c superconductivity	<5 meV

common magnetic materials occurs on a similar energy scale so that such studies can be easily accomplished at ordinary light sources.

In some ways graphene is exceptional in that good results can be measured with only modest energy resolution. In Fig. 2, the Dirac energy as well as the optical phonon and plasmon energy scales are large (up to a couple hundred meV) and so the measurements are typically limited not by energy resolution but by sample quality and beamline flux. But as the doping level is reduced, the Dirac energy and the plasmon energy scale are both continuously reduced until they overlap with the electron–phonon kink near the Fermi level. Studying the mutual electron–electron–phonon interaction therefore requires a much finer energy discrimination.

Other ground states, such as conventional, high-temperature and exotic superconductivity, typically involve yet smaller energy scales such as acoustic phonon or magnon modes. In principle these degrees of freedom extend down to zero energy scale, which explains the low phase transition temperatures to these ground states. Studies of these effects demand not only higher energy resolution but also sample temperature control down to a few Kelvin.

2.2. Spatial resolution

It was already hinted above that self-organized or engineered materials display fluctuations of the electronic properties (including many-body correlations) on the submicrometer spatial scales; it is clear that [as proposed by Smith & Kevan (1991)] it is of tremendous advantage to have a probe at the same spatial scales to determine these position-dependent properties.

Spectromicroscopy using photoemission developed at various synchrotrons first on the basis of core level measurements (using scanning photoemission microscopy, or SPEM), and followed more recently by efforts to build angle- and energy-resolving experiments capable of determining the spectral function $A(\mathbf{k}, \omega)$. Depending on the photon spot size achieved, such scanning instruments can be called ‘ μ ARPES’ or ‘nARPES’ for the micrometer or nanometer length scale, respectively. Such machines are either already operating [at synchrotrons Elettra (Barbo *et al.*, 2000; Dudin *et al.*, 2010) and Soleil (Avila *et al.*, 2013c,b; Avila & Asensio, 2014)], are currently being commissioned [at ALS (Rotenberg, 2010; Bostwick *et al.*, 2012)] or are in various stages of planning worldwide (e.g. Diamond, NSLS-2, Petra III, SSRL, *etc.*).

Fig. 3 shows a schematic of the forthcoming nanoARPES end-station currently being commissioned at the MAESTRO beamline at the ALS (Bostwick *et al.*, 2012). In order to focus the X-rays to a small spot at the sample, it is necessary to demagnify the source by the ratio of the desired spot size to the source size (determined by the monochromator exit aperture). Since the exit slits operate in the range of tens of micrometers, it requires a demagnification factor of around 1000 to achieve a spot size on the order of tens of nanometers. Since the sample is of the order of 1–2 m away from the source, it requires that the focusing optics must be within a few millimeters of the sample.

Currently the most cost-effective way to achieve small spot sizes is through the use of diffractive optics such as the Fresnel zone plate (ZP) or related technologies such as photon sieves (Kipp *et al.*, 2001). These are patterned diffractive optics with overall size in the millimeter range but with individual features on the nanometer scale. Because they demagnify the X-rays by using convergence of diffracted light, an order-sorting aperture (OSA) is placed between the ZP and the sample in order to reject unwanted diffracted orders. Depending on the ZP parameters, the OSA may have to be placed quite close to the sample, limiting both the access of the detector to the emitted electrons, as well as the capabilities (for example, heating and cooling) of the sample holder. These problems have been addressed in three ways: (i) by scaling up the overall size of the instrument (requiring larger ZPs and more floorspace, at higher cost) (Avila *et al.*, 2013c); (ii) by reducing the size of the OSA and ZP positioning systems through miniaturization (requiring greater engineering effort, also at higher cost) (Bostwick *et al.*, 2012); and (iii) by using reflective schemes such as Schwarzschild optics (requiring expensive optics) (Barbo *et al.*, 2000).

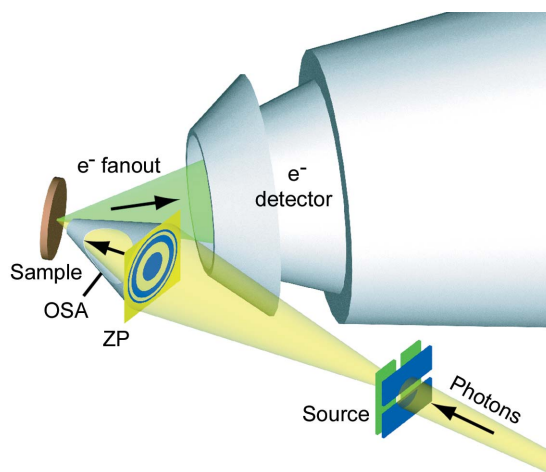


Figure 3

Detection scheme for nanoARPES. The photon source (typically the exit slit of a monochromator) illuminates a Fresnel zone plate (ZP), which is imaged onto the sample. Reduction of stray diffraction orders requires an order-sorting aperture (OSA) which is here schematically shown as a cone. The application of photons to the sample induces a photoelectron cloud, a portion of which (the e^- fan-out cone) is collected by an electron lens coupled to an electron hemispherical analyzer (not shown). [Reproduced from Rotenberg (2010).]

The development of nanoARPES was realised in the mid-2000s, with the earliest ARPES band maps acquired with submicrometer spatial resolution being published around 2010 (Rotenberg, 2010; Usachov *et al.*, 2011), and the technique has been gradually building momentum with many publications since (Frantzeskakis *et al.*, 2012; Avila *et al.*, 2013a; Bignardi *et al.*, 2013; Cattelan *et al.*, 2013; Wilson *et al.*, 2013; Johansson *et al.*, 2014). Considering that the days of development and proof-of-principle studies are now behind us, together with the multiplication of instruments around the world, a great acceleration in the rate of publications using nanoARPES can be expected in the next couple years.

It should be noted that there is a complementary technique, spatially resolved photoemission electron microscopy (PEEM), which has also been successfully used to acquire ARPES band maps of a few layers of graphene (Sutter *et al.*, 2009). Despite the many advantages of PEEM microscopy (such as the ability to use the same instrument to monitor real-time growth of samples, and the rapid survey capability with superior spatial resolution), it is difficult to achieve spectral resolutions better than about $100 \text{ meV}/2 \mu\text{m}/1^\circ$ in ARPES mode, which are all of the order ten times worse than can be achieved with scanning-spot machines. Hence, in general, many-body physics is not accessible with PEEMs (although there has been a notable study of electron–electron interaction effects in graphene (Knox *et al.*, 2011). [It should also be noted that PEEMs are subject to space-charge effects, discussed in detail below for ARPES, which can lead to both loss of spatial and spectral resolutions (Locatelli *et al.*, 2011).]

Not surprisingly, most of the publications cited above have been studies of graphene or graphite, partly because of the tremendous recent interest in these and other Dirac materials, and partly because of the ease of preparing these samples (they can be prepared *ex situ* and transferred through the air with minimal *in situ* treatment), and also because they are extremely resistant to radiation-induced damage that follows as a consequence of small-spot focusing. It should be noted, however, that extreme radiation-hardness is not a fundamental requirement and that there have been successes in studies of oxides using both scanning PES (Sarma *et al.*, 2004; Lupi *et al.*, 2010) and nanoARPES (Frantzeskakis *et al.*, 2012). The ability to determine the many-body interactions in oxides with spectromicroscopic ARPES opens up vast fields of study of correlated oxides (Shenoy *et al.*, 2006).

3. Ultimate ARPES performance at DL light sources

A fundamental limitation on the energy and angle resolution of ARPES is scattering among the emitted electrons, the so-called space-charge broadening effect. This effect has been routinely observed or predicted for pulsed-light based ARPES such as at third-generation light sources and in laser-based setups (Zhou *et al.*, 2005; Passlack *et al.*, 2006; Hellmann *et al.*, 2009, 2012; Buckanie *et al.*, 2009; Graf *et al.*, 2010). These studies show, not surprisingly, that reducing the illumination spot size or reducing the incoming pulse length rapidly increase the broadening due to space-charge effects. However,

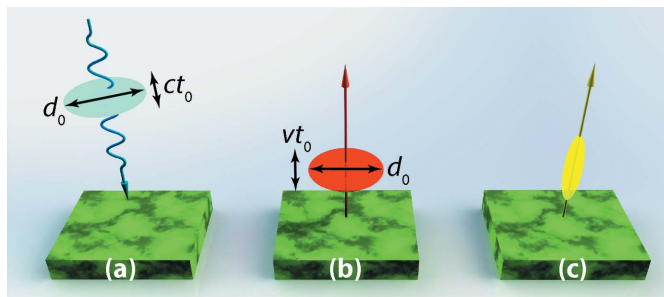


Figure 4

Time and space scales in ARPES. (a) The incoming photon pulse and (b, c) the outgoing electron cloud for short-pulse and nanoARPES regimes, respectively. The in-plane length scale d_0 and the pulse length t_0 of the light pulse sets the in-plane and normal dimensions of the electron clouds.

as Hellmann *et al.* have shown theoretically, and experiments have borne out, these effects cannot increase indefinitely but are bounded.

Fig. 4 schematically illustrates the space and time scales that need to be considered in calculations of the space-charge broadening (Hellmann *et al.*, 2009, 2012) (for clarity, only electrons emitted at normal angles are included in the illustration). The incoming photon pulse [Fig. 4(a)] has in- and out-of-plane dimensions d_0 and ct_0 , which set the corresponding dimensions of the space-charge cloud [Figs. 4(b) and 4(c)], d_0 and vt_0 . Here we can take v to be the average velocity of the electrons, which are distributed in energy from zero to the photon energy (within the value of the work function).

The two regimes illustrated in Figs. 4(b) and 4(c) represent the short-pulse ($d_0 \gg vt_0$) and small-spot ($d_0 \ll vt_0$) limits. Following Hellmann *et al.* (2009, 2012) we consider these limits in turn. Starting from a mixed regime ($d_0 \simeq vt_0$) and reducing the spot size, one will eventually reach a regime where the space-charge cloud dimensions are effectively one-dimensional in the normal direction. The electron–electron interactions can then depend only on the pulse length, and further reduction in spot size cannot increase the space-charge broadening. Similarly, starting from the mixed regime and reducing the pulse length, one eventually reaches a regime where the space-charge cloud is two-dimensional, and the interactions are governed only by the spot size. Reducing the pulse length cannot increase the space-charge interactions further.

These scaling arguments show that both time-resolved and spatially resolved ARPES, while subject to space charge, are not impossible, although the space-charge broadening does indeed increase without bounds when *both* d_0 and t_0 are simultaneously reduced.

Simulations of space-charge broadening are heavily dependent upon the material parameters, mainly through the penetration depth of the photons, the escape depth of the electrons, the dielectric strength of the material, and the energy and angular distributions of the electrons (Zhou *et al.*, 2005). An exact calculation of the space-charge broadening is also difficult for large numbers of electrons, and approxima-

tions have to be made. An adaptive cell approach by Hellmann *et al.* has been successfully used to approximate the fully interacting cloud and compares well with measured broadening; we have found a simple approximation that is easy to implement yields similar values for space-charge broadening.

In our calculation, which uses physical parameters of gold as an example, we generate a population of cloud electrons distributed within the solid according to the penetration depth of the light and allow the electrons to propagate outwards. The energy distribution is generated according to the measured gold photoemission spectrum, and the angle distribution is assumed isotropic. At $t = 0$ (chosen randomly during the photon pulse) a test charge is emitted from the surface in the normal direction. In subsequent time steps, the test charge is allowed to interact with the cloud. Forces on the test charge cause its path to deflect and its energy to increase or decrease according to the details of the randomly chosen trajectories. The energy broadening of the test charge is computed from the distribution of results after some hundreds of simulation runs are performed. The time steps were systematically reduced until the calculation converged. Following the previous cited calculations, screening due to the sample substrate was taken into account using the image charge method. We assumed that the image charge has the same magnitude as the electron (infinite dielectric constant approximation).

An important aspect of the calculations is that the test charge energy is always chosen to be at the Fermi level E_F . This reflects the fact that in ARPES we are interested in the valence band and not the core levels. Because the test charge has the maximum kinetic energy of the cloud electrons, it can quickly overtake and escape from the bulk of the cloud, and when it does so it can no longer be scattered. Therefore, we can expect that space-charge broadening is minimal for electrons near the Fermi level compared with deeper core-electrons, which is a good thing for determination of the many-body interactions, since these involve long-lived charge carriers near the Fermi level for which high energy resolution is most desirable.

In many cases there is a large population of electrons just below the Fermi level; for example, oxides typically have a very large number of electrons distributed about 6 eV below the Fermi edge; therefore gold was chosen as a prototype material due to the similar large distribution of $5d$ electrons near E_F . This shows that simple materials like aluminium will have less space-charge broadening than gold or oxide samples, and so we have chosen gold as a prototype as something of a worse-case scenario.

Two simplifying approximations are made to make the calculations more efficient. First, the cloud electrons do not interact with each other. Second, the test charge's path is allowed to be deflected by the cloud electrons, but the cloud electrons are not deflected by the test charge. Both of these assumptions are conservative, because by making these assumptions we are increasing the net effect on the test charge. Therefore the computed energy broadening must be an upper limit to the actual broadening. Nevertheless we have found

our calculated energy broadenings to be similar to those of the previous authors.

Fig. 5 shows calculated values of energy broadening ΔE due to space-charge scattering for 80 eV photon energy for two different spot sizes: (a) 10 μm and (b) 50 nm. These calculations are carried out as a function of photon pulse duration (t_0) and number of electrons per pulse (N_e). The latter is determined by the storage ring, beamline and material parameters,

$$N_e = \Phi \times \text{QE}/f, \quad (4)$$

where Φ [photons s^{-1}] is the beamline flux, QE is the quantum efficiency for photoelectron production, and f is the repetition rate of the storage ring. As discussed in the next section, N_e varies in the range from a few to a few hundred for a third-generation non-diffraction-limited light source such as the ALS.

The photon energy chosen for calculations (80 eV) was chosen as a compromise between the desire for lower photon energy (where kinematic constraints improve both photon energy resolution and the outgoing momentum resolution)

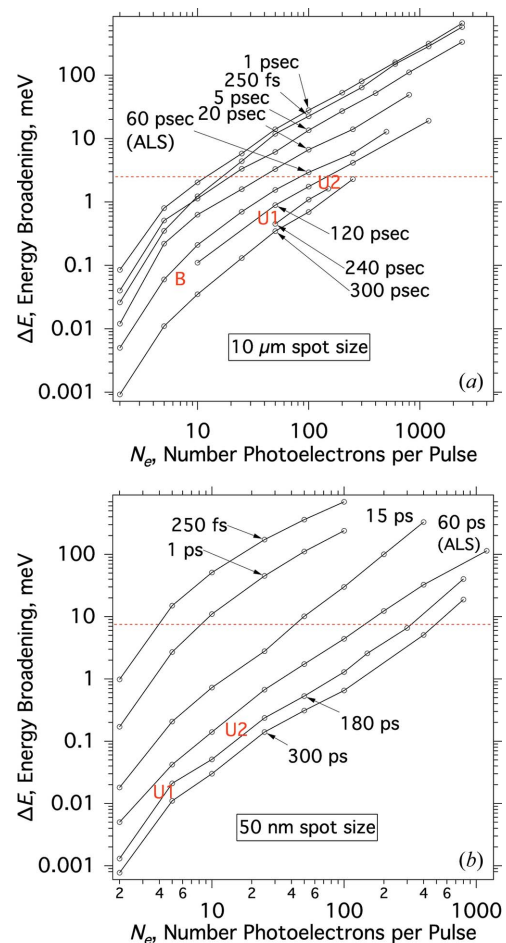


Figure 5 Space-charge calculations for (a) 10 μm and (b) 50 nm spot sizes, as a function of number of electrons generated per soft X-ray pulse, and as a function of soft X-ray pulse duration (full width at half-maximum). The calculations are for 80 eV photon energy. The labels B, U1 and U2 mark the positions of the baseline ALS performance, and the improved performance under two different upgrade scenarios as discussed in the text.

and higher photon energy (which provides for smaller diffraction-limited spot sizes due to the decreasing photon wavelength). It is difficult, with such ‘back of the envelope’ calculations that we are presenting, to precisely assess the photon energy dependence of the space-charge effect, because the photoelectron energy distribution varies with kinetic energies and we do not have a simple model of such effects, which depend on material parameters.

We merely note that, while space-charge broadening increases at lower energies (due to the decreasing energy difference between the valence electrons and the low-energy tail of the photoelectron distribution), on the other hand the functionality of nanoARPES is diminished because diffraction-limited spot size increases inversely with energy. If one is willing to deal with a larger spot size, then the increased spot size will counteract the increase in space-charge broadening, which should therefore not increase too badly with decreasing energy. With respect to space-charge broadening effects in conventional ARPES at 10 μm focus, whether or not it is beneficial to use lower photon energy will depend very much on material parameters and has to be assessed experimentally on a case-by-case basis.

In addition to energy broadening, angular broadening due to space-charge scattering has also been demonstrated in the cited calculations, as well as ours. Present electron spectrometers are limited in our experience to an angle resolution of around 0.1° which is dominated by two limiting effects: imaging aberrations in the electron optics and the finite resolution of micro-channel plate detectors. The former could be addressed in principle with better lens quality and alignment precision, but the latter cannot be improved without significant detector improvements, or else scaling up the size of the electron analyzers.

Fig. 6 shows the correlation between energy and angular broadening for 50 nm and 10 μm spot sizes, for various pulse

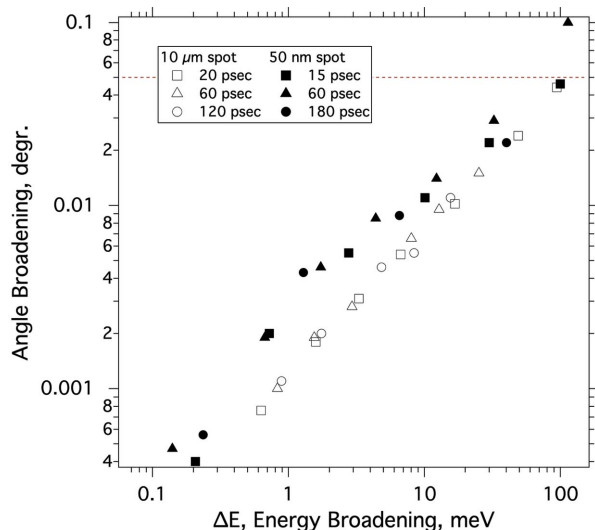


Figure 6 Relationship between angle and energy broadening for various photon pulse lengths and fluxes for 10 μm (open symbols) and 50 nm (closed symbols) spot sizes. The dashed line is the threshold (0.05°) for unacceptable angular broadening.

lengths and photon fluxes. Hellman *et al.* (2009) has demonstrated that, for conventional ARPES, energy broadening becomes a problem well before angular broadening reaches this level. Our calculations agree with this conclusion not only for ARPES but for nanoARPES. Fig. 6 shows that each meV of energy broadening corresponds to only about one milli-degree of angular broadening, independent of photon pulse length and N_e , and only modestly sensitive to spot size. In practice we would like to keep angular broadening below 0.05° (dashed line in Fig. 6), which is easily achieved even up to energy broadening of ~ 100 eV.

4. Discussion

We seek to operate in a condition where ΔE is some factor, say 0.5, of the chosen energy resolution, so that the net resolution (source + ΔE) is increased by only a modest (12%) factor. To give a definite example, consider a microARPES measurement at the MAESTRO beamline (Warwick & Reininger, 2010) where the beamline is set to 5 meV energy resolution at 80 eV, yielding a 10 μm spot size. The expected flux is $\Phi = 2.2 \times 10^{12}$ at 20000 resolving power at 80 eV; f is about 500 MHz; for gold, the QE is about 1%. So we can expect a cloud of 44 electrons generated per pulse in a standard (non-focused) ARPES experiment. For 5 meV resolution, the acceptable broadening limit $\Delta E = 2.5$ meV is indicated by the dashed line in Fig. 5(a).

For spectromicroscopy, we must consider the effects of focusing the X-rays to a small spot, and two cases are discussed.

4.1. Case 1: microARPES at ALS beamline 7

The present ALS electron beam is nearly diffraction-limited in the vertical direction, but is far from this limit in the horizontal direction; therefore the X-rays are focused onto an asymmetric 10 μm (V) \times 40 μm (H) spot at the sample. So in order to achieve a symmetric 10 μm spot, it is required to aperture down the beamline at the exit slit plane, and therefore the cloud size is reduced by about a factor of six (the coherent fraction) to a baseline rate of about $N_e \simeq 7$ electrons per bunch. Since the ALS pulse length at the moment is 60 ps FWHM, this locates the baseline performance of MAESTRO μ ARPES [‘B’ symbol in Fig. 5(a)]. Since the energy broadening in this situation is only 1 meV, we conclude that space-charge broadening will be negligible compared with the 10 meV resolution.

In an upgraded DL-ALS, there are two scenarios currently under consideration. Exploiting *Advantage 1* of §2, the beam will become fully diffraction-limited in both the horizontal and vertical directions, and at the same time the pulse length of the ALS will be increased by up to a factor of three. These changes imply, importantly, that the horizontal aperture at the monochromator exit plane will no longer be overfilled, leading to a flux increase of the order of the change in coherence (increases by a factor of six). At the same time, the space-charge effect is diminished because of the lengthening of the

ALS pulse. So the space-charge broadening increases by only a factor of two [‘U1’ in Fig. 5(a)].

In the second upgrade scenario, the insertion device is optimized for a smaller vacuum chamber (*Advantage 2* in §2). In this scenario, we can estimate an additional gain in flux of a factor of 3.5. This takes us to a fully optimized condition [‘U2’ in Fig. 5(a)]. Any further gains in flux will not be possible at this spatial resolution without space-charge broadening becoming significant. This means that increasing the insertion device length will not offer any special advantages, unless either the spatial and/or energy resolution requirements are relaxed, or else the pulse length of the light source can be extended. Considering that the beamline flux is roughly linear with the desired resolution, and that space-charge broadening is roughly linear with the photon flux in this regime, then this conclusion will be true for any energy resolution requirement above 0.5 meV or so.

4.2. Case 2: nanoARPES at ALS beamline 7

We now consider how upgrade of the ALS to a diffraction-limited light source affects nanoARPES. Calculations of the energy broadening ΔE due to space-charge effects is shown in Fig. 5(b). We need to choose a grating and aperture size in order to just fill our zone plate focusing optic, whose diameter is 750 μm . This is accomplished by using a 60 μm aperture at the monochromator’s exit slit plane, which is located 2 m upstream of our zone plate optics. These settings will give an effective energy resolution of 15 meV, so our goal in order to avoid space-charge broadening is to limit ΔE to 7.5 meV.

The μARPES baseline rate of 7 electrons per bunch needs to be modified for nanoARPES to account for the efficiency of the zone plate (optimistically 10%), so with 0.7 electrons per bunch we are well into the non-degenerate limit (≤ 1 electron per pulse) where $\Delta E \rightarrow 0$.

In the first upgrade scenario (U1, DL only) discussed above, the rate of electron generation increases by a factor of six, but still stays close to the non-degenerate limit so that ΔE remains negligible. The fact that the pulse length in the DL-ALS increases is not important because the charge density remains low.

Even in the second upgrade scenario (U2, DL + new insertion device) the space-charge broadening remains negligible. This shows that there is much room in the nanoARPES technique for improvement, either by using a longer insertion device, shorter periods or more advanced concepts for high field devices such as cryogenically cooled magnets. Such improvements will greatly aid the flux without introducing significant space-charge broadening.

5. Conclusion and caveats

Emergent phenomena at the mesoscale arise because of the many complex interactions between the degrees of freedom in the solid. ARPES is an especially good experimental probe of these interactions, and so it is important to extend ARPES to

a spectromicroscopic technique in order to understand the origins of these spatially varying properties.

DL light sources provide a considerable improvement (of the order of a factor of 20) in performance over the previous generation, and it was shown in this report that, for micrometer-scale focused X-ray beams at high energy resolution, optimized performance of the microARPES technique can be achieved with modest-sized insertion devices. By optimum, it is meant that further increases in flux cannot be sustained without energy broadening become important. For nanoARPES, space-charge limitations are not particularly important in DL light sources, even with very long high-flux insertion devices (longer than are presently available at the ALS).

There are two important caveats, however, before we blithely apply these happy conclusions:

First, nanoARPES, as implemented using diffractive (zone-plate-based) optics is shown to be photon-flux limited at the ALS (which has modest insertion device size with length ~ 2 m), even after an upgrade of the storage ring to DL performance. Therefore a nanoARPES end-station will benefit by careful selection of insertion device in order to maximize flux. Not discussed above though, is the issue of thermal loading of the sample, which may impose an important additional limitation on the incident flux. This has two effects: increase of the local sample temperature and damage of the sample by inducing vacancy or defect formation. A back-of-the-envelope calculation (and indeed practical experience) shows that, for samples of sufficiently high thermal conductivity and under conditions of low absorption, temperature rise is not severe, but for other materials, especially near absorption edges where the photon flux is absorbed close to the surface, we can anticipate both larger temperature increases. Depending on the material and photon energy, defect formation will always be possible.

Second, we mentioned above that the space-charge broadening depends strongly on material parameters which were not explored here. This can be an important factor in characterizing materials displaying phase changes. For example, a metal-to-insulator transition can lead to a substantial reduction in the screening properties of the substrate, increasing the space-charge broadening (up to a factor of two could be expected). Such an increase would be associated with an apparent broadening of the spectrum which should not be construed as intrinsic to the phase transition. What is perhaps more worrying is the associated shift of the energy spectrum due to the space charge. These shifts, typically to higher kinetic energy, are of the same order as the energy broadening, and will strongly impact the determination of quantities such as energy gap *versus* temperature at the Fermi level, especially for sharp transitions at which material properties are fluctuating quickly.

Both of these effects can be characterized by changing the photon flux, and reducing it if necessary until they become negligible. Since beam damage is not uncommon at the previous generation light sources, this is already a common practice in ARPES. Certainly there are samples that already

do not work well for ARPES with respect to beam damage, and this situation can only become worse for nanoARPES; nevertheless, the results so far are promising.

The Advanced Light Source is supported by the Director, Office of Science, Office of Basic Energy Sciences, of the US Department of Energy under Contract No. DE-AC02-05CH11231. The authors thank S. D. Kevan for critically reading the manuscript.

References

- Avila, J. & Asensio, M. C. (2014). *Synchrotron Radiat. News*, **27**, 24–30.
- Avila, J., Razado, I., Lorcy, S., Fleurier, R., Pichonat, E., Vignaud, D., Wallart, X. & Asensio, M. C. (2013a). *Sci. Rep.* **3**, 2439.
- Avila, J., Razado-Colambo, I., Lorcy, S., Giorgetta, J.-L., Polack, F. & Asensio, M. C. (2013b). *J. Phys. Conf. Ser.* **425**, 132013.
- Avila, J., Razado-Colambo, I., Lorcy, S., Lagarde, B., Giorgetta, J.-L., Polack, F. & Asensio, M. C. (2013c). *J. Phys. Conf. Ser.* **425**, 192023.
- Barbo, F., Bertolo, M., Bianco, A., Cautero, G., Fontana, S., Johal, T. K., La Rosa, S., Margaritondo, G. & Kaznatcheyev, K. (2000). *Rev. Sci. Instrum.* **71**, 5–10.
- Bignardi, L., van Dorp, W. F., Gottardi, S., Ivashenko, O., Dudin, P., Barinov, A., De Hosson, J. T. M., Stöhr, M. & Rudolf, P. (2013). *Nanoscale*, **5**, 9057–9061.
- Bostwick, A., Rotenberg, E., Avila, J. & Asensio, M. C. (2012). *Synchrotron Radiat. News*, **25**, 19–25.
- Bostwick, A., Speck, F., Seyller, T., Horn, K., Polini, M., Asgari, R., MacDonald, A. H. & Rotenberg, E. (2010). *Science*, **328**, 999–1002.
- Buckanie, N. M., Göhre, J., Zhou, P., von der Linde, D., Hoegen, M. H.-v. & Heringdorf, F.-J. M. z. (2009). *J. Phys. Condens. Matter*, **21**, 314003.
- Cattelan, M., Agnoli, S., Favaro, M., Garoli, D., Romanato, F., Meneghetti, M., Barinov, A., Dudin, P. & Granozzi, G. (2013). *Chem. Mater.* **25**, 1490–1495.
- Chiang, T. C. (2000). *Surface Sci. Rep.* **39**, 181–235.
- Damascelli, A. (2004). *Phys. Scr.* **T109**, 61–74.
- Damascelli, A. & Shen, Z.-X. (2003). *Rev. Mod. Phys.* **75**, 473–541.
- Dudin, P., Lacovig, P., Fava, C., Nicolini, E., Bianco, A., Cautero, G. & Barinov, A. (2010). *J. Synchrotron Rad.* **17**, 445–450.
- Frantzeskakis, E., Avila, J. & Asensio, M. C. (2012). *Phys. Rev. B*, **85**, 125115.
- Graf, J., Hellmann, S., Jozwiak, C., Smallwood, C. L., Hussain, Z., Kaindl, R. A., Kipp, L., Rossnagel, K. & Lanzara, A. (2010). *J. Appl. Phys.* **107**, 014912.
- Hellmann, S., Ott, T., Kipp, L. & Rossnagel, K. (2012). *Phys. Rev. B*, **85**, 075109.
- Hellmann, S., Rossnagel, K., Marczyński-Bühlow, M. & Kipp, L. (2009). *Phys. Rev. B*, **79**, 035402.
- Hemminger, J., Crabtree, G. & Sarrao, J. (2012). *From Quanta to the Continuum: Opportunities for Mesoscale Science*. US Department of Energy Technical Report, <http://science.energy.gov/bes/news-and-resources/reports/>.
- Hu, Y. F., Zuin, L., Wright, G., Igarashi, R., McKibben, M., Wilson, T., Chen, S. Y., Johnson, T., Maxwell, D., Yates, B. W., Sham, T. K. & Reininger, R. (2007). *Rev. Sci. Instrum.* **78**, 083109.
- Hüfner, S. (1996). *Photoelectron Spectroscopy*. Berlin: Springer-Verlag.
- Johansson, L. I., Armiento, R., Avila, J., Xia, C., Lorcy, S., Abrikosov, I. A., Asensio, M. C. & Virojanadara, C. (2014). *Sci. Rep.* **4**, 4157.
- Kaminski, A. & Fretwell, H. M. (2005). *New J. Phys.* **7**, 98.
- Kevan, S. D. (1992). *Angle-Resolved Photoemission: Theory and Current Applications*, Vol. 74. Amsterdam: Elsevier.
- Kipp, L., Skibowski, M., Johnson, R. L., Berndt, R., Adelung, R., Harm, S. & Seemann, R. (2001). *Nature (London)*, **414**, 184–188.
- Knox, K. R., Locatelli, A., Yilmaz, M. B., Cvetko, D., Menteş, T. O., Niño, M. A., Kim, P., Morgante, A. & Osgood, R. M. (2011). *Phys. Rev. B*, **84**, 115401.
- Locatelli, A., Menteş, T. O., Niño, M. A. & Bauer, E. (2011). *Ultramicroscopy*, **111**, 1447–1454.
- Lundqvist, B. (1967a). *Phys. Kondens. Mater.* **6**, 193–205.
- Lundqvist, B. (1967b). *Phys. Kondens. Mater.* **6**, 206–217.
- Lundqvist, B. (1968). *Phys. Kondens. Mater.* **7**, 117–123.
- Lupi, S., Baldassarre, L., Mansart, B., Perucchi, A., Barinov, A., Dudin, P., Papalazarou, E., Rodolakis, F., Rueff, J. P., Itié, J. P., Ravy, S., Nicoletti, D., Postorino, P., Hansmann, P., Parragh, N., Toschi, A., Saha-Dasgupta, T., Andersen, O. K., Sangiovanni, G., Held, K. & Marsi, M. (2010). *Nat. Commun.* **1**, 105.
- Passlack, S., Mathias, S., Andreyev, O., Mitnacht, D., Aeschlimann, M. & Bauer, M. (2006). *J. Appl. Phys.* **100**, 024912.
- Rotenberg, E. (2010). *X-rays in Nanoscience: Spectroscopy, Spectromicroscopy and Scattering Techniques*, edited by Jinghua Guo, ch. 6, pp. 169–206, *Many-Body Interactions in Nanoscale Materials by Angle-Resolved Photoemission Spectroscopy*. Weinheim: Wiley-VCH.
- Sarma, D., Topwal, D., Manju, U., Krishnakumar, S., Bertolo, M., La Rosa, S., Cautero, G., Koo, T., Sharma, P., Cheong, S. W. & Fujimori, A. (2004). *Phys. Rev. Lett.* **93**, 097202.
- Shenoy, V. B., Sarma, D. D. & Rao, C. N. R. (2006). *ChemPhysChem*, **7**, 2053–2059.
- Smith, K. E. & Kevan, S. D. (1991). *Prog. Solid State Chem.* **21**, 49–131.
- Sutter, P., Hybertsen, M. S., Sadowski, J. T. & Sutter, E. (2009). *Nano Lett.* **9**, 2654–2660.
- Temnykh, A. (2008). *Phys. Rev. ST Accel. Beams*, **11**, 120702.
- Usachov, D., Vilkov, O., Gruneis, A., Haberer, D., Fedorov, A., Adamchuk, V. K., Preobrajenski, A. B., Dudin, P., Barinov, A., Oehzelt, M., Laubschat, C. & Vyalikh, D. V. (2011). *Nano Lett.* **11**, 5401–5407.
- Valla, T., Kralj, M., Siber, A., Milun, M., Pervan, P., Johnson, P. D. & Woodruff, D. P. (2000). *J. Phys. Condens. Matter*, **12**, L477–L482.
- Warwick, T. & Reininger, R. (2010). Technical Report LSBL982RevA. Advanced Light Source, Lawrence Berkeley National Laboratory, Berkeley, CA, USA.
- Wilson, N. R., Marsden, A. J., Saghier, M., Bromley, C. J., Schaub, R., Costantini, G., White, T. W., Partridge, C., Barinov, A., Dudin, P., Sanchez, A. M., Mudd, J. J., Walker, M. & Bell, G. R. (2013). *Nano Res.* **6**, 99–112.
- Zhou, X. J., Wannberg, B., Yang, W. L., Brouet, V., Sun, Z., Douglas, J. F., Dessau, D., Hussain, Z. & Shen, Z. X. (2005). *J. Electron Spectrosc. Relat. Phenom.* **142**, 27–38.